JACC: BASIC TO TRANSLATIONAL SCIENCE VOL. 4, NO. 8, 2019

PRECLINICAL RESEARCH

Preservation of Post-Infarction Cardiac Structure and Function via Long-Term Oral Formyl Peptide Receptor Agonist Treatment

Ricardo A. García, PhD,[a,b] Bruce R. Ito, PhD,[b] John A. Lupisella, MSc,[a] Nancy A. Carson, BSc,[a] Mei-Yin Hsu, MSc,[a] Gayani Fernando, MSc,[a] Madeleine Heroux, PhD,[c] Michel Bouvier, PhD,[c] Elizabeth Dierks, PhD,[a] Ellen K. Kick, PhD,[a] David A. Gordon, PhD,[a] Jian Chen, PhD,[a] Gabe Mintier, BSc,[a] Marilyn Carrier, PhD,[c] Stéphane St-Onge, MSc,[c] Himanshu Shah, MSc,[a] Jordan Towne, BSc,[b] Marcela Sotelo Bucardo, BSc,[b] Xiuying Ma, PhD,[a] Carol S. Ryan, BSc,[a] Nicholas R. Wurtz, PhD,[a] Jacek Ostrowski, PhD,[a] Francisco J. Villarreal, MD, PhD[b]

VISUAL ABSTRACT

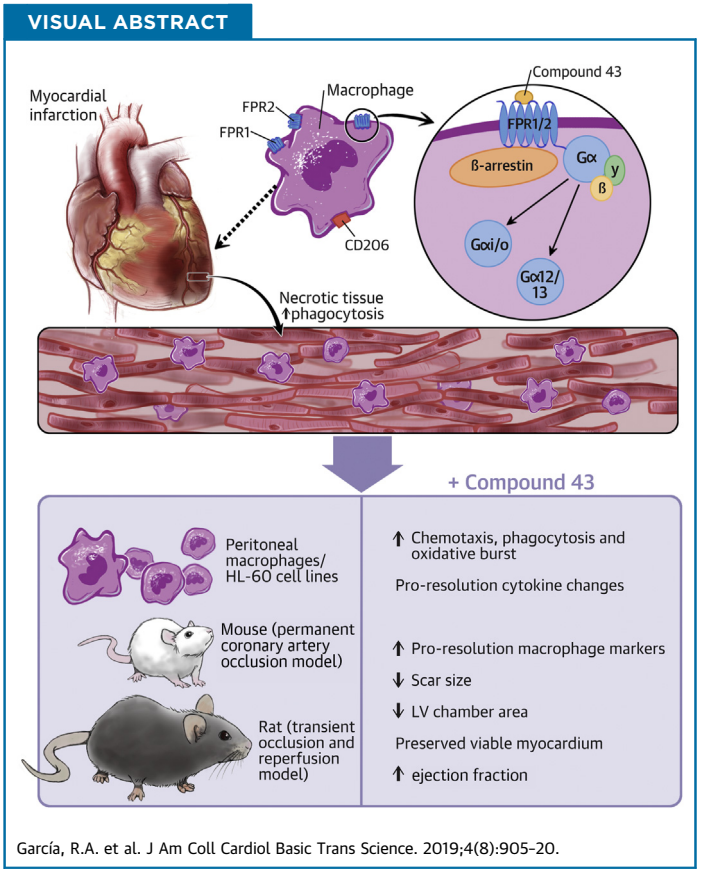

García, R.A. et al. J Am Coll Cardiol Basic Trans Science. 2019;4(8):905-20.

HIGHLIGHTS

- **Myocardial infarction leads to recruitment of monocyte/macrophages to the injured myocardium to drive infarct healing.**
- **Activation of formyl peptide receptors (FPR1 and FPR2) present on macrophages contributes to key cellular activities that can potentiate wound healing.**
- **Myocardial infarction was induced in rodents to study the effects of long-term treatment with Compound 43, a small molecule agonist of FPR1 and FPR2.**

ISSN 2452-302X https://doi.org/10.1016/j.jacbts.2019.07.005

JACC: BASIC TO TRANSLATIONAL SCIENCE VOL. 4, NO. 8, 2019
DECEMBER 2019:905–20

ABBREVIATIONS AND ACRONYMS

Cmpd43 = Compound 43
FPR = formyl peptide receptor
HF = heart failure
IL = interleukin
IR = ischemia-reperfusion
KO = knockout
LAD = left anterior descending
LV = left ventricular
MI = myocardial infarction
PV = pressure-volume
SAA = serum amyloid A
WT = wild-type

- **Main findings: Compound 43 stimulated proresolution macrophage activities, improved left ventricle and infarct structure, and preserved cardiac function post-myocardial infarction.**
- **The results suggest that stimulation of proresolution activities of FPRs can favorably alter post-myocardial infarction pathophysiology that leads to heart failure.**

SUMMARY

Dysregulated inflammation following myocardial infarction (MI) promotes left ventricular (LV) remodeling and loss of function. Targeting inflammation resolution by activating formyl peptide receptors (FPRs) may limit adverse remodeling and progression towards heart failure. This study characterized the cellular and signaling properties of Compound 43 (Cmpd43), a dual FPR1/FPR2 agonist, and examined whether Cmpd43 treatment improves LV and infarct remodeling in rodent MI models. Cmpd43 stimulated FPR1/2-mediated signaling, enhanced proresolution cellular function, and modulated cytokines. Cmpd43 increased LV function and reduced chamber remodeling while increasing proresolution macrophage markers. The findings demonstrate that FPR agonism improves cardiac structure and function post-MI.

Heart failure (HF) is a leading cause of morbidity and mortality in the United States, affecting up to 5.7 million people (1). Myocardial infarction (MI) remains a prevalent cause of HF, with up to 25% of patients with MI developing the disease. Despite advances in pharmacotherapy, HF-associated mortality remains high, and the development of new therapeutic approaches is needed.

The early sequelae of events following MI include a localized inflammatory response that resolves in a coordinated manner to enable myocardial healing and scar formation. Unresolved inflammation is responsible for the pathophysiology of multiple, diverse chronic diseases, such as atherosclerosis and HF (2). In the MI setting, persistent unresolved inflammation is a major contributor to the progressive development of adverse left ventricular (LV) remodeling and eventually HF. However, early attempts to mitigate inflammation following MI using relatively nonspecific agents, such as glucocorticoids (3,4) or cyclooxygenase-2 inhibitors (5,6), have been unsuccessful and led to major adverse events, including LV rupture. An alternative strategy to address post-MI inflammation involves the promotion of resolution to improve healing of the damaged myocardium and its restoration to homeostasis. The discovery of proresolving lipid mediators (e.g., lipoxins and resolvins) and their cognate receptors, including formyl peptide receptor (FPR) 2, has opened new opportunities for pharmacological treatment of unresolved inflammation (7).

FPRs are G–protein-coupled receptors that are prominently expressed by phagocytic leukocytes, including macrophages, and play important roles in the initiation and resolution of inflammation. FPR1 and FPR2 are the most characterized isoforms in the FPR family, and both bind structurally diverse ligands. The stimulation of FPR2 has been shown to modulate the post-MI healing response via the polarization of macrophages to a proresolution phenotype, sometimes referred to as “M2” (8,9). In

From the [a]Department of Cardiovascular and Fibrosis Drug Discovery, Bristol-Myers Squibb Company, Pennington, New Jersey; [b]Department of Medicine, University of California San Diego, San Diego, California; and the [c]Institute for Research in Immunology and Cancer, Université de Montréal, Montréal, Québec, Canada. This work was supported by Bristol-Myers Squibb (Princeton, NJ, USA). Bristol-Myers Squibb policy on data sharing may be found at https://www.bms.com/researchers-andpartners/independent-research/data-sharing-request-process.html. All other authors have reported that they have no relationships relevant to the contents of this paper to disclose.
The authors attest they are in compliance with human studies committees and animal welfare regulations of the authors’ institutions and Food and Drug Administration guidelines, including patient consent where appropriate. For more information, visit the *JACC: Basic to Translational Science* author instructions page.

Manuscript received February 22, 2019; revised manuscript received July 16, 2019, accepted July 17, 2019.

addition, treatment with the endogenous ligands resolvin D1 and 15-epi-lipoxin promotes inflammation resolution and limits early remodeling (8,9). Similar observations have been made with a synthetic FPR1/2-biased agonist that demonstrated cardioprotective properties when given at the time of myocardial injury (10).

SEE PAGE 921

To address the capacity of FPRs to provide long-term benefit after myocardial injury, a dual agonist of FPR1/2 identified as Compound 43 (Cmpd43) (11–13) was administered orally to evaluate relationships between heart structure and function after MI. In addition, the signaling and cellular response stimulated by Cmpd43 and regulation of key cytokines associated with proinflammatory and pro-resolution phases are described.

METHODS

For an expanded Methods section, please see the Online Appendix.

IN VITRO AND/OR CELLULAR ASSAYS. The dose-response activity of Cmpd43 on intracellular signaling and key inflammatory cell functions, including phagocytosis, oxidative burst, chemotaxis, and cytokine gene expression, was determined in peritoneal macrophages or established cell lines (HL-60 or HEK293).

The signaling profile of Cmpd43 was determined in HEK293 cells that transiently expressed either FPR1 or FPR2. Activation of G proteins (Gαi1, Gαi2, Gαi3, GαoA, GαoB, Gα12, and Gα13) and recruitment of β-arrestins (β-arrestin-1 and β-arrestin-2) were measured using bioluminescence resonance energy transfer–based biosensor assays (14).

Phagocytosis was evaluated using BioGel-elicited peritoneal macrophages from wild-type (WT) C57BL/6 mice and FPR1 and FPR2 knockout (KO) mice. The FPR2 KO was analogous to that reported by Dufton et al. (15), which was deficient in FPR2 and FPR3 (see Online Appendix). Macrophages were treated with Cmpd43 for 15 min and provided with opsonized fluorescein isothiocyanate-labeled zymosan (1:8 ratio of cells to zymosan) for 45 min at 37°C. Phagocytosis was quantified using a fluorescence plate reader.

Cellular oxidative burst, which occurs in phagocytes following zymosan uptake, was measured in differentiated HL-60 cells and engineered CRISPR KO HL-60 cells deficient in FPR1 or FPR2. Cells were incubated for 15 min in buffer containing 0.4 mM luminol and a concentration range of Cmpd43 before stimulation with 2 μg of opsonized zymosan. Bioluminescence was quantified immediately after stimulation using a plate reader.

Chemotaxis in HL-60 cells was assessed using Transwell plates. Migration was induced by placing Cmpd43 in the bottom chamber and HL-60 cells in the top. Cells were allowed to migrate into the lower chamber for 120 min and then quantified using a cell viability assay.

Regulation of cytokine gene expression in BioGel-elicited peritoneal macrophages was evaluated in the setting of proinflammatory stimulation using serum amyloid A (SAA). SAA is an acute-phase protein secreted during the early inflammatory response and is a ligand for various receptors, including FPR2 (16). Macrophages were pre-treated with Cmpd43 for 30 min followed by incubation for 5 h ± 600 nM SAA. Cells were lysed directly in Tri Reagent, and mRNA levels of inflammatory cytokines interleukin (IL)-10 and IL-6 were quantified by reverse transcription polymerase chain reaction.

ANIMAL STUDIES

Animal studies followed American Association for Accreditation of Laboratory Animal Care guidelines, and protocols were approved by Bristol-Myers Squibb and University of California San Diego Animal Care and Use committees. Adult male C57BL/6 mice (10 to 12 weeks old) and adult male Sprague-Dawley rats (6 to 7 weeks old) were purchased from the Jackson Laboratory (Bar Harbor, Maine) and Charles River Laboratories (Wilmington, Massachusetts), respectively.

Animals were anesthetized with an intraperitoneal injection of ketamine (100 mg/kg) and xylazine (8 mg/kg) followed by endotracheal intubation and mechanical ventilation with oxygen supplemented with isoflurane (2.0% to 2.5%). The heart was exposed surgically via a left thoracotomy. In mice, the left anterior descending (LAD) artery was permanently occluded by suture. In rats, ischemia-reperfusion (IR) was implemented by transiently occluding the LAD artery for 45 min. For sham animals, a suture was placed but not tightened. The chest was closed and appropriate analgesics administered. In the mouse MI study, the treatment groups were sham (n = 14), MI vehicle (0.5% carboxymethylcellulose) (n = 13), MI Cmpd43 (1 mg/kg) (n = 14), and MI Cmpd43 (10 mg/kg) (n = 14). Once-daily oral dosing by gavage was initiated 24 h post-MI and continued for 4 weeks. An independent set of treated mice (n = 4 to 8) were euthanized approximately 3 days post-MI, and hearts were harvested 2 h after dosing for macrophage marker assays as described in the following section. In the rat IR experiments, treatment groups were

FIGURE 1 Signaling Profile of Cmpd43 in HEK293 Cells Expressing Human FPR1 and FPR2

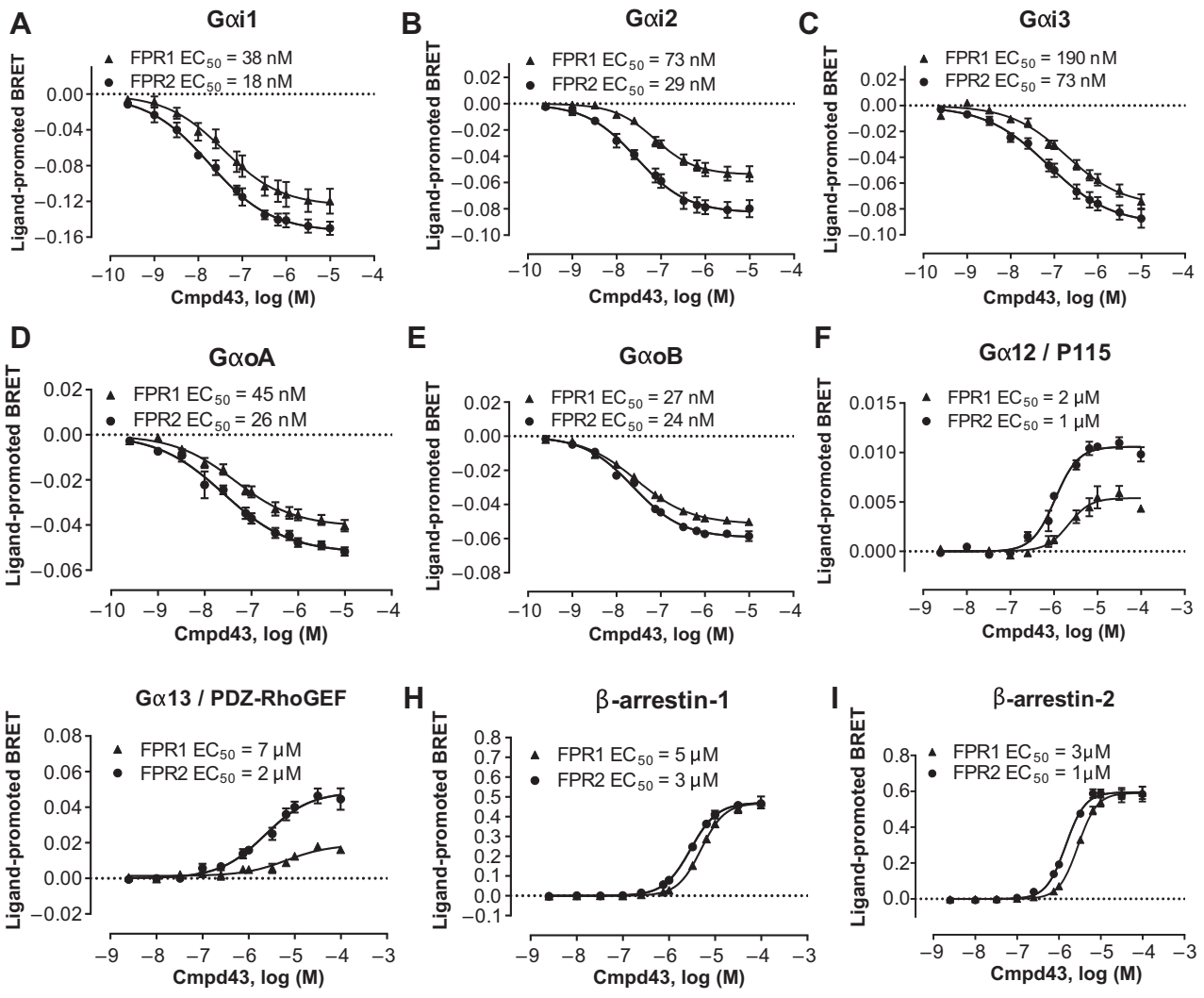

The ability of Compound 43 (Cmpd43) to engage different signaling pathways was assessed using bioluminescence resonance energy transfer (BRET) biosensors that detected the activation of **(A)** Gαi1, **(B)** Gαi2, **(C)** Gαi3, **(D)** GαoA, and **(E)** GαoB, the interaction of effectors with **(F)** Gα12 and **(G)** Gα13, as well as the recruitment of **(H)** β-arrestin-1 and **(I)** β-arrestin-2 to the plasma membrane. HEK293 cells expressing human formyl peptide receptor (FPR)-1 or FPR2 were stimulated with Cmpd43, and modulation of the BRET signals from the different biosensors was recorded. Data represent the mean ± SEM of 3 independent experiments. EC_{50} = concentration of Cmpd43 that gives half-maximal response.

sham (n = 10), MI vehicle (n = 17), and MI Cmpd43 (10 mg/kg) (n = 14). Once-daily oral dosing by gavage was initiated 48 h post-MI and continued for 6 weeks.

In terminal studies, LV pressure-volume (PV) relationships (mouse and rat) and passive 2-dimensional epicardial strains of the infarct scar (mouse) were measured ex vivo in diastolic-arrested and excised mouse and rat hearts. Using a Langendorff apparatus, the aorta was cannulated for perfusion with diastolic arrest buffer. A thin-walled balloon was placed into the LV cavity and connected to a pressure transducer and infusion pump. Epicardial surface markers were placed on the anterior epicardial wall. A digital camera was positioned to capture images of the scar or analogous region of sham hearts. LV inflation-deflation conditioning cycles were followed by 2 to 3 acquisition runs. Synchronized video images were obtained. Subsequently, hearts were perfusion fixed with 10% buffered formalin while maintaining LV balloon pressure at 10 to 15 mm Hg. Hearts were stored in formalin for histological processing. In the rat terminal

FIGURE 2 Regulation of Inflammatory Cell Function by Cmpd43

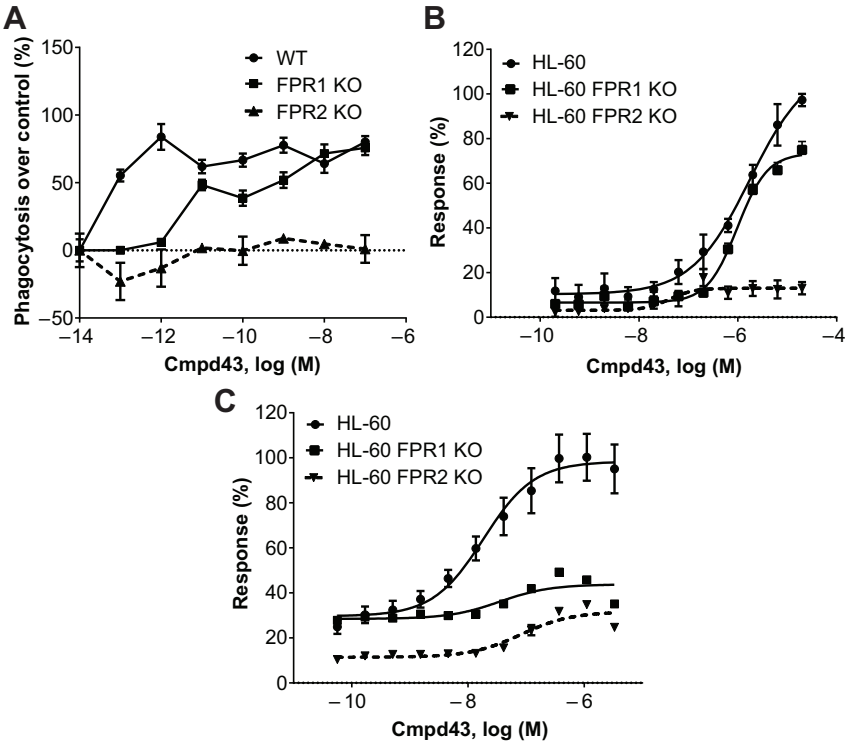

(A) Enhancement of zymosan phagocytosis by Cmpd43 was assessed in BioGel-elicited peritoneal macrophages from wild-type (WT), FPR1 knock out (KO), and FPR2 KO mice. **(B)** Stimulation of oxidative burst activity was evaluated in neutrophil-like HL-60, HL-60 FPR1 KO, and HL-60 FPR2 KO cell lines. **(C)** Chemotactic responses to Cmpd43 were evaluated in HL-60, HL-60 FPR1 KO, and HL-60 FPR2 KO cell lines. Other abbreviations as in Figure 1.

experiments at 6 weeks post-IR, animals were re-anesthetized with isoflurane, and a transducer-tipped conductance catheter (2.5-F; Millar, Inc., Houston, Texas) was inserted into the left ventricle via a right carotid cutdown. LV PV loop data were acquired and corrected for parallel conductance using the bolus intravenous saline injection method. Volume calibration was performed with rat blood against known volumes using standardized cuvettes. PV loop data were analyzed using LabChart software (AD Instruments, Inc., Colorado Springs, Colorado). Rat hearts were subsequently excised following diastolic arrest, and ex vivo passive PV curves were obtained as described previously for mice.

MACROPHAGE PHENOTYPING. Two h after the last Cmpd43 dose, mice were injected intraperitoneally with 100 U of heparin and then anesthetized with 5% isoflurane. Hearts were removed, minced into pieces, and digested with a mild collagenase cocktail for 35 min. The cell suspension was filtered to remove debris, and residual red blood cells were lysed. Samples (2×10^6 cells) were processed for flow cytometry using the following surface markers: CD45 [PerCP], Ly-6G[APC-Cy7], CD64[APC], and CD206[PE-Cy7]. Data were analyzed post hoc.

HISTOLOGY. Hearts were cut along the short axis at the midventricle and processed. Paraffin-embedded sections were cut and stained with trichrome or picrosirius red for collagen evaluation and analyzed by computer-assisted histomorphometry for quantitation of scar area and left ventricle cavity and myocardial wall dimensions. In situ hybridization experiments were carried out to detect arginase-1 and FPR2 mRNA levels in the peri-infarct border zone of mouse hearts. The target mRNAs were visualized using a standard bright field microscope and scanned at 20× using the Aperio eSlide Manager (Leica Biosystems Imaging, Inc., Vista, California) followed by quantitation.

DATA AND STATISTICAL ANALYSIS. Statistical significance was determined using a Student's *t*-test or analysis of variance followed by a Dunnett's post hoc

FIGURE 3 IL-10 and IL-6 Regulation by Cmpd43

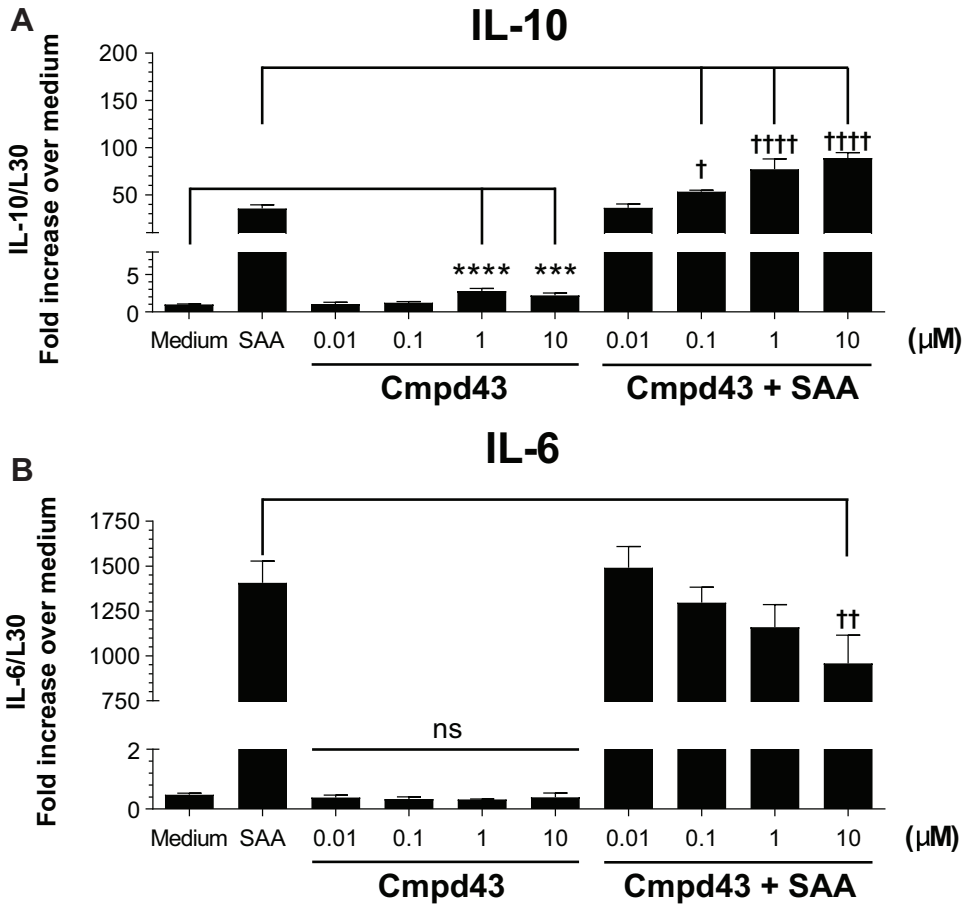

Concentration-dependent regulation of **(A)** interleukin (IL)-10 and **(B)** IL-6 mRNA levels by Cmpd43 in BioGel-elicited mouse peritoneal macrophages. Macrophages were pretreated with Cmpd43 for 30 min followed by incubation for 5 h ± 600 nM serum amyloid A (SAA). **(C)** IL-10 and **(D)** IL-6 mRNA modulation in peritoneal macrophages from WT and FPR2 KO mice are presented. Data represent the mean ± SEM. Dunnett's versus medium: **$p < 0.01$, ***$p < 0.001$, ****$p < 0.0001$. Dunnett's versus SAA: †$p < 0.05$, ††$p < 0.01$, †††$p < 0.001$, ††††$p < 0.0001$. Other abbreviations as in Figures 1 and 2.

Continued on the next page

test to compare specified treatments with a single control. Statistical analyses were conducted, and values for the concentration of Cmpd43 that gives half-maximal response (EC_{50}) were calculated using GraphPad Prism Version 7.03 (GraphPad Software, Inc., La Jolla, California). Unless otherwise noted, data are shown as mean ± SEM. Statistical significance was noted as $p < 0.05$, $p < 0.01$, $p < 0.001$, or $p < 0.0001$.

RESULTS

The first objective was to evaluate the cellular properties of Cmpd43. The signaling profile was examined in HEK293 cells that expressed human FPR1 or FPR2. Cmpd43 produced concentration-dependent modulation of bioluminescence resonance energy transfer signals for Gαi1, Gαi2, Gαi3, GαoA, and GαoB biosensors following FPR1 and FPR2 activation (EC_{50} shown in Figures 1A to 1E). The responses for the Gαi/o signaling pathways were consistent with FPR1 and FPR2 agonist-mediated reductions in cellular cyclic adenosine monophosphate (17,18). A response was also observed for Gα12 and Gα13 biosensors after stimulation of FPR1- or FPR2-expressing cells with Cmpd43 (Figures 1F and 1G), but not for Gαq, Gα11, or Gαs biosensors (Online Figure 1). This

FIGURE 3 Continued

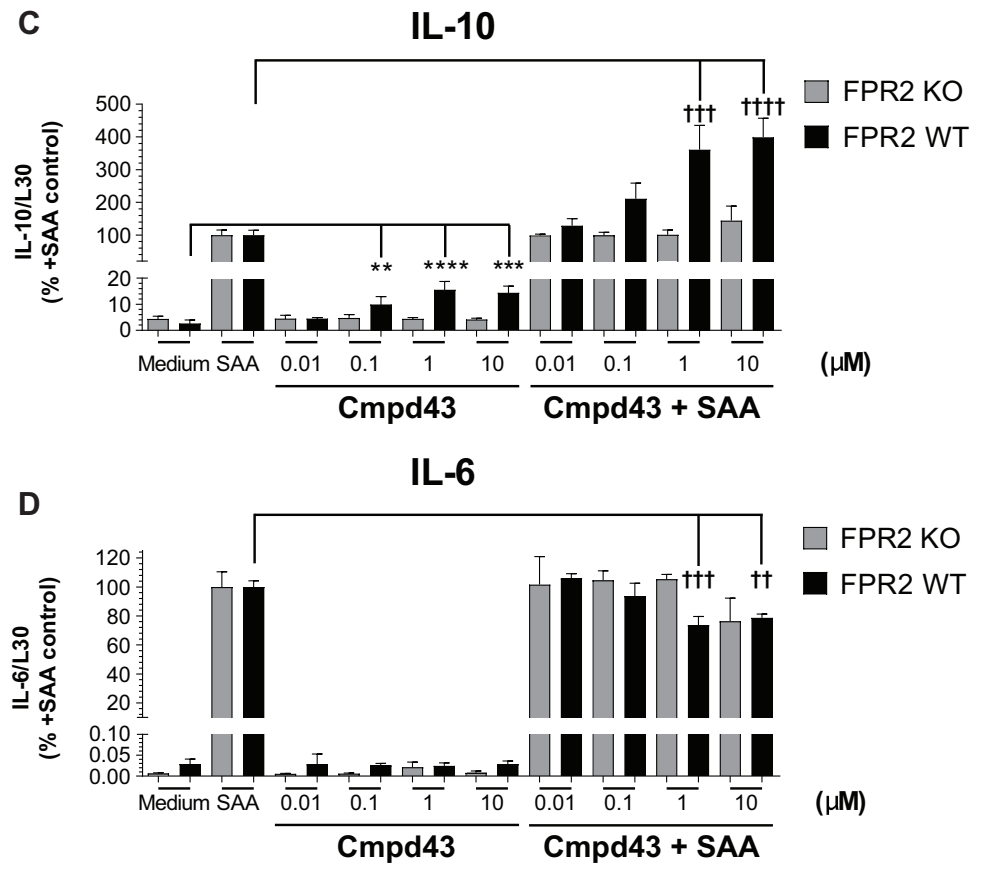

observation suggested that in addition to coupling to Gαi/o family members, FPR1 and FPR2 could also engage Gα12 and Gα13 proteins after stimulation with Cmpd43. Cmpd43 also promoted β-arrestin-1 and -2 recruitment to both FPR1 and FPR2 (**Figures 1H and 1I**). The potency values for β-arrestin-1 and -2 recruitment, as well as for Gα12 and Gα13 activation, were consistently reduced for both receptor subtypes compared with the Gαi/o signaling pathways, with EC_{50} values between 1 and 7 μM for the β-arrestins and Gα12/13 signaling pathways, as opposed to 18 to 190 nM for Gαi/o activation. Bioluminescence resonance energy transfer assays were also carried out using rat and mouse FPR2 receptors and confirmed activation of the Gi pathway as well as recruitment of β-arrestin-1 to rodent species with Cmpd43 (Online Figure 2). Overall, the signaling profile of Cmpd43 was conserved between FPR1 and FPR2, with both receptor subtypes leading to Gαi/o, Gα12/13, and β-arrestin-1 and -2 activation after Cmpd43 stimulation.

Zymosan phagocytosis was evaluated in peritoneal macrophages from WT, FPR1 KO, and FPR2 KO mice. As shown in **Figure 2A**, potent stimulation of phagocytosis with Cmpd43 occurred with WT-derived macrophages (EC_{50} ~0.1 pM) with an apparent plateau achieved at 1 pM. By contrast, FPR2 KO–derived macrophages did not respond to Cmpd43 stimulation above control. FPR1 KO–derived macrophages showed an intermediate response, which suggested a modest role of FPR1 in phagocytosis enhancement.

Phagocytes respond to chemotactic stimuli and degrade internalized particles and bacteria while undergoing an oxidative respiratory burst (19). The capacity of Cmpd43 to stimulate oxidative burst activity and chemotaxis was investigated using differentiated human promyelocytic leukemia HL-60 cells, which possess a neutrophil-like lineage (20). **Figure 2B** shows Cmpd43-stimulated oxidative burst activity in HL-60 (EC_{50} = 1.8 μM) and HL-60 FPR1 KO (EC_{50} = 1 μM) cells. Activity was essentially abolished in the HL-60 FPR2 KO line. Cmpd43 also stimulated

FIGURE 4 Arginase-1 and CD206 Levels Post-MI

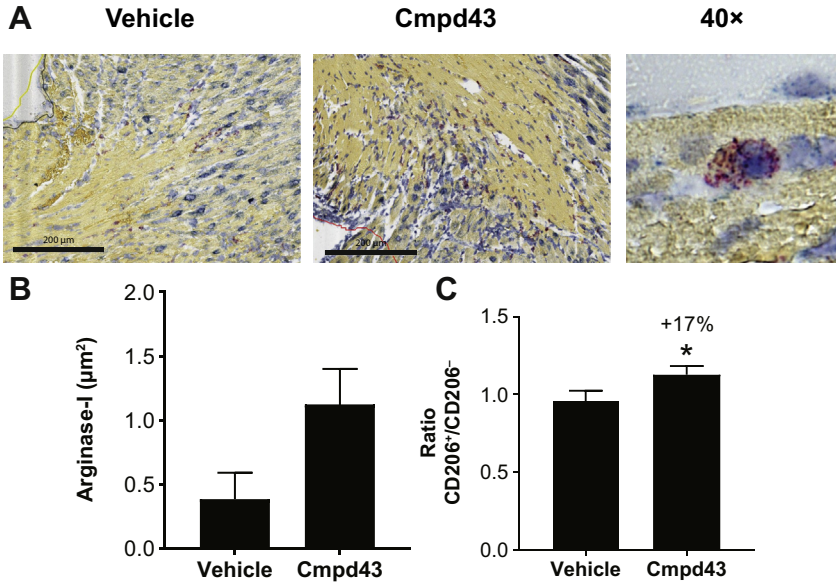

(A) Histologic images of arginase-1 by in situ hybridization 74 h following myocardial infarction (MI) via permanent left coronary artery ligation. Representative images of the peri-infarct zone from infarcted mice treated with vehicle or Cmpd43 (10 mg/kg) are shown. Arginase-1 mRNA is indicated in **red** and FPR2 mRNA is **blue**. A 40× image of a macrophage containing arginase-1 and FPR2 is shown on the **right**. **(B)** Quantification of arginase-1 mRNA levels for vehicle and Cmpd43 (10 mg/kg; n = 4 per group). **(C)** Ratio of $CD206^{+}/CD206^{-}$ macrophages from infarcted mice treated with vehicle (n = 9) or Cmpd43 (10 mg/kg; n = 10). Whole hearts were digested and cell homogenates were analyzed by flow cytometry. *t*-test: *$p < 0.05$. Other abbreviations as in Figures 1 and 2.

chemotaxis of differentiated HL-60 cells with an EC_{50} of 18 nM (Figure 2C). Absence of FPR1 and FPR2 severely impaired chemotactic responses, which suggested both isoforms were involved.

The cytokines IL-10 and IL-6 are induced during inflammation and resolution processes (21). As shown in Figure 3, Cmpd43 modulated the expression levels of these cytokines in peritoneal macrophages. In the absence of proinflammatory stimulation with SAA, Cmpd43 alone increased IL-10 gene expression approximately 2- to 3-fold at 1 and 10 μM relative to medium control ($p < 0.001$) (Figure 3A). When macrophages were treated with 600 nM SAA, IL-10 mRNA increased 35-fold versus medium. In the presence of Cmpd43, IL-10 levels were increased 1.5-, 2.2-, and 2.5-fold at 0.1, 1, and 10 μM relative to SAA control, respectively. In the same experiment, induction of IL-6 mRNA expression with SAA was significantly attenuated in the presence of Cmpd43 10 μM ($p < 0.05$) (Figure 3B). To confirm that the changes in expression of these cytokines were due, in part, to agonism of FPR2 with Cmpd43, a parallel experiment was conducted with peritoneal macrophages from FPR2 KO mice and WT littermates. In the absence of FPR2, no modulation of IL-10 or IL-6 mRNA expression was observed either with Cmpd43 alone or in the presence of SAA (Figures 3C and 3D).

To determine whether Cmpd43 activity on macrophage function observed in vitro would manifest under MI conditions in vivo, the early effects of Cmpd43 on macrophages were evaluated in mouse cardiac tissue after MI. Arginase-1, a canonical marker for M2 proresolution macrophages (22), was evaluated in a small cohort of mice (n = 4 per group) approximately on day 3 following MI (2 h after the third dose of Cmpd43). Histologic images showed increases in arginase-1 mRNA via in situ hybridization (Figure 4A). A trend toward increased levels of arginase-1 was observed with Cmpd43 relative to vehicle in the peri-infarct border zone (~4-fold vs. vehicle) (Figure 4B). No apparent difference in total macrophage content between treatment groups was observed (Online Figure 3). A comparative experiment with a larger cohort was conducted to detect global changes in proresolution markers in the whole heart. CD206 represents another classic marker of proresolution macrophages (22). Using the same in-life protocol, CD206 surface levels were assessed

FIGURE 5 Cmpd43 Effects on LV and Infarct Structure 28 Days Post-MI in Mice

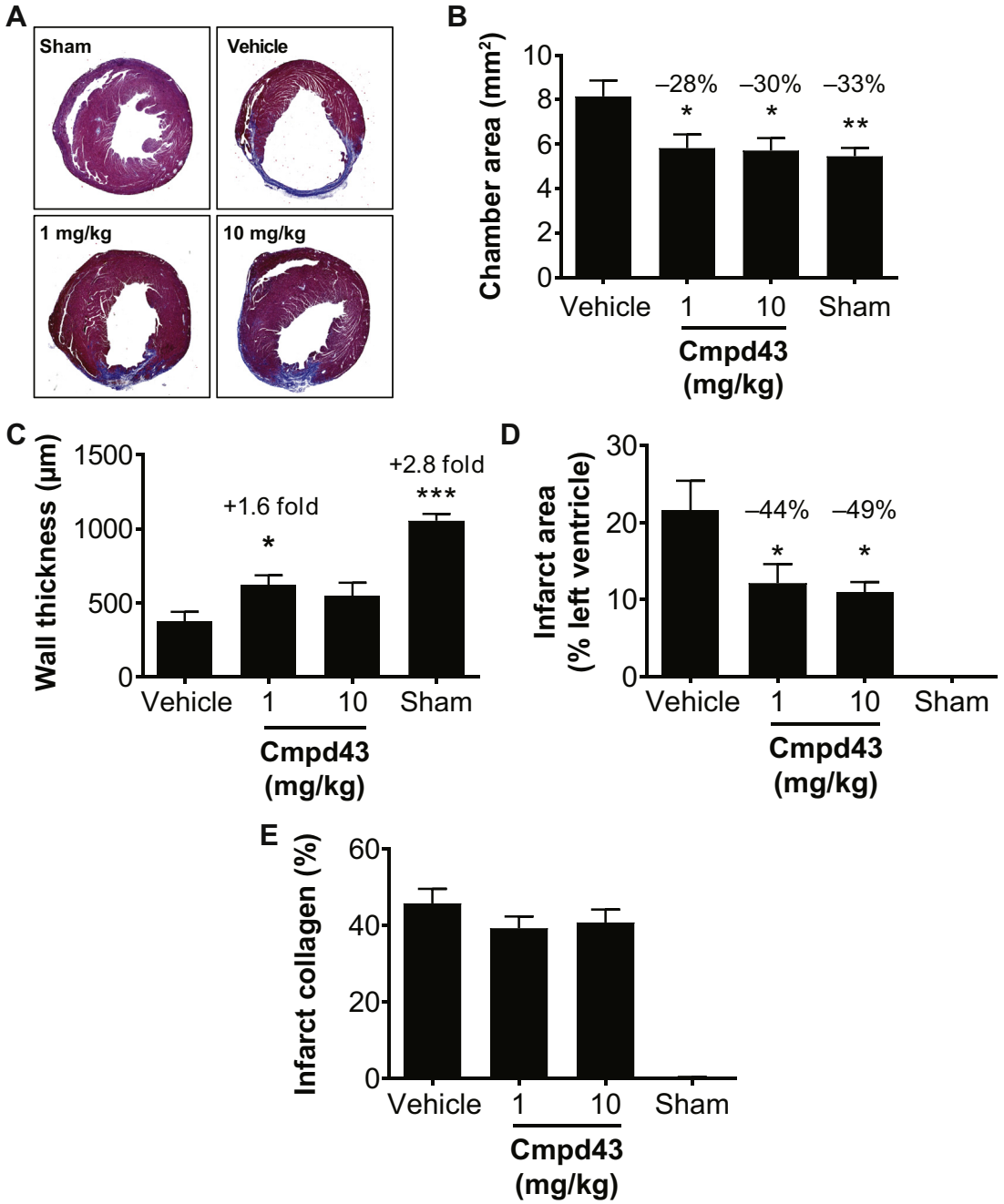

Treatments were initiated 24 h after MI and continued to 28 days. Treatments consisted of a suspension vehicle and Cmpd43 at either 1 mg/kg or 10 mg/kg. **(A)** Representative heart cross sections by histology depicting the degree of MI. Noninfarcted surgical sham animals are shown for comparison. Histomorphometric analysis of **(B)** chamber area, **(C)** infarct wall thickness, **(D)** infarct area, and **(E)** infarct collagen content 28 days after MI. Dunnett's versus vehicle: *$p < 0.05$, **$p < 0.01$, ***$p < 0.001$. Other abbreviations as in Figures 1, 2, and 4.

FIGURE 6 Mouse LV Passive Mechanics and 2-Dimensional Epicardial Scar Strains 28 Days Post-MI

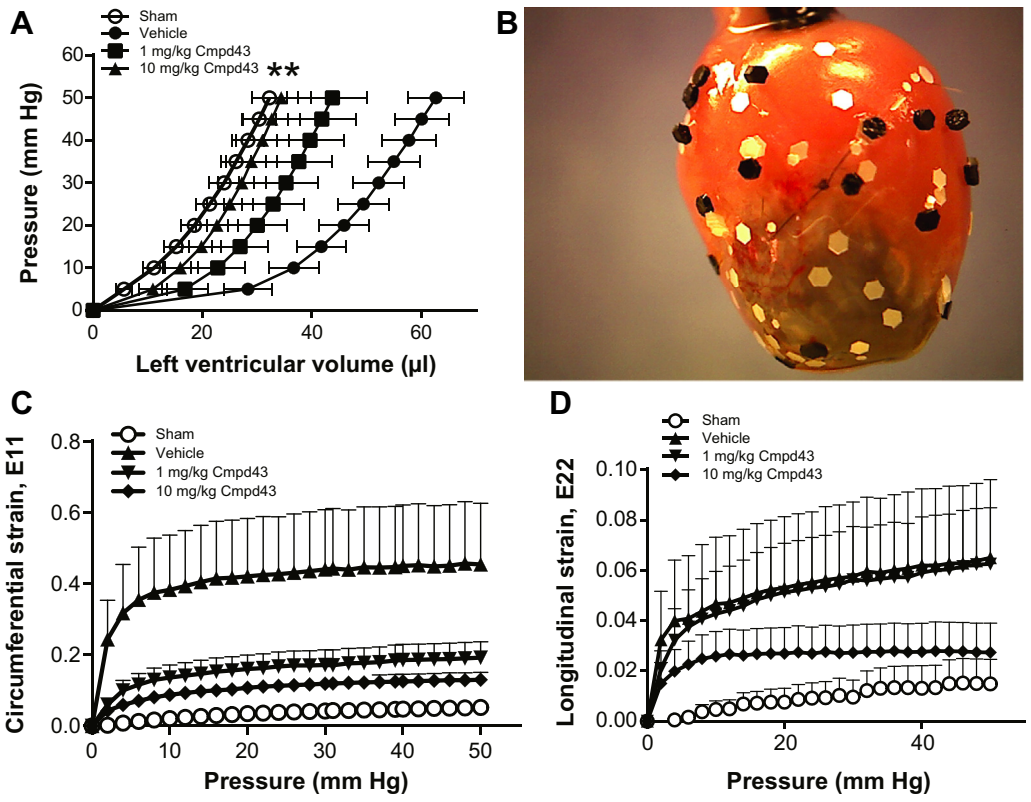

(A) LV pressure–volume curves. **(B)** Representative mouse heart preparation for epicardial scar strains analysis showing marker placement on the heart. **(C)** Circumferential (E_{11}) scar strains. **(D)** Longitudinal (E_{22}) scar strains. One-way analysis of variance (all pressures): **$p < 0.01$. Abbreviations as in Figures 1, 4, and 5.

in macrophages isolated from post-MI hearts following mild collagenase digestion and flow cytometry. The ratio of pro-resolution $CD206^+$ macrophages was increased 17% in mice treated with Cmpd43 versus vehicle ($p < 0.05$) (Figure 4C). No significant difference in $CD64^+$ macrophage content between treatment groups was detected (Online Figure 3).

The effects of a 28-day treatment with Cmpd43 (1 and 10 mg/kg QD, orally) on LV and infarct scar remodeling were evaluated in the mouse permanent coronary artery occlusion model. Cross sections of the heart were analyzed for histomorphometric assessments of LV chamber area, scar dimensions (size and wall thickness), and infarct collagen content. Figure 5A shows representative cross sections of trichrome-stained hearts for the various treatment groups and shams. The extent of chamber dilatation, wall thinning, and infarct scar in the treated groups was visually less than that in the vehicle group. Figure 5B shows the effects of treatments on chamber dilatation. Treatment with Cmpd43 attenuated chamber expansion at the 1 and 10 mg/kg doses (−28 and −30% vs. vehicle, respectively; $p < 0.05$). The chamber areas for Cmpd43-treated mice were similar in size to noninfarcted shams. Infarct wall thicknesses were measured for all groups (Figure 5C). The 1 mg/kg Cmpd43 dose yielded a 1.6-fold increase in wall thickness relative to vehicle ($p < 0.05$). A trend toward increased wall thickness was noted at the 10 mg/kg dose versus vehicle. In addition, there were no differences in contralateral wall thicknesses between treatment groups (Online Figure 4). Infarct scar area was measured and reported as a percentage of the total LV cross-sectional area. Cmpd43 reduced LV anterior wall infarct scar size at 1 and 10 mg/kg doses (44% and 49% relative reductions vs. vehicle, respectively; $p < 0.01$) (Figure 5D). Notably, no differences in infarct collagen content were observed between treatment groups (Figure 5E), indicating no

FIGURE 7 Cmpd43 Effects on Cardiac Structure/Function Following Ischemia–Reperfusion in the Rat

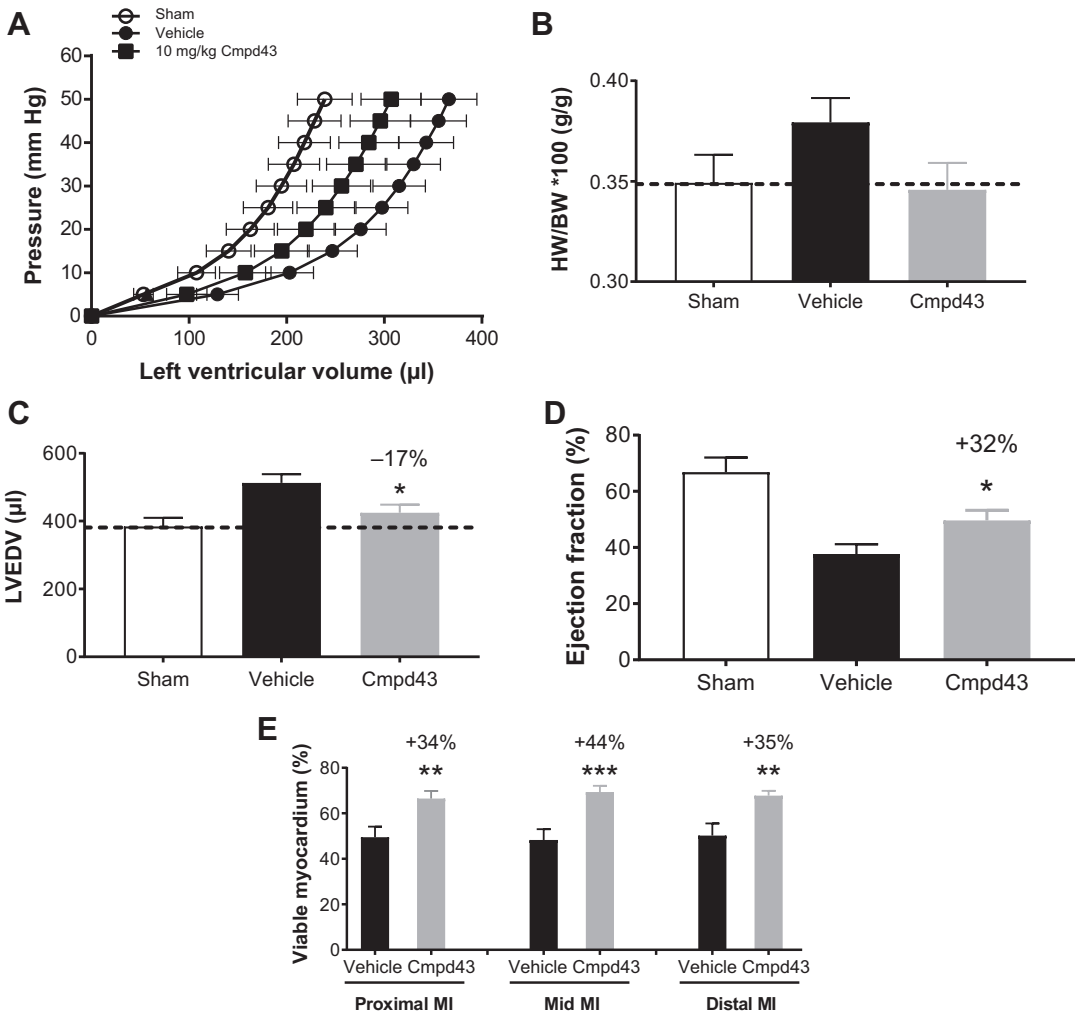

(A) LV pressure–volume curves, **(B)** heart weight (HW)/body weight (BW) ratio, **(C)** left ventricular end-diastolic volume (LVEDV), **(D)** ejection fraction, and **(E)** percent viable myocardium relative to infarct scar across the infarcted wall (epicardium to endocardium) at the proximal MI region near the ligature, at the mid-MI region, and at the distal MI region. Dunnett's versus vehicle: *$p < 0.05$, **$p < 0.01$, ***$p < 0.001$. Other abbreviations as in Figures 1, 4, and 5.

adverse impact on infarct collagen deposition and wound healing after MI.

The effect of Cmpd43 on ex vivo LV passive mechanics 28 days post-MI was consistent with the previously described histomorphometric data (Figure 6A). Compared with noninfarcted sham hearts, there was a pronounced rightward shift in the PV curve of the MI vehicle group. By contrast, PV curves obtained with Cmpd43 were left-shifted relative to vehicle ($p < 0.01$), which indicated smaller LV chamber volumes versus vehicle. At the 10 mg/kg dose, the PV curve was comparable to the sham PV curve. At the 1 mg/kg dose, the curve was left-shifted to an intermediate level between the sham and vehicle. Epicardial scar strains were measured for all groups (Figure 6B). Scar strain measurements along the short axis of the heart (circumferential E_{11} direction) are shown in Figure 6C. Sham hearts were analyzed in a region of the left ventricle where infarction was predicted to occur. For the sham group, E_{11} strains were small (i.e., stiff myocardium). By contrast, vehicle showed the highest scar strains in the E_{11} direction, which suggested an

TABLE 1 LV Hemodynamics Data 6 Weeks Post-Ischemia-Reperfusion Injury

	Sham	Vehicle	Cmpd43
Heart rate, beats/min	308.5 ± 7.6	316.0 ± 5.1	303.2 ± 8.1
Pao systolic, mm Hg	129.8 ± 5.5	125.1 ± 3.5	124.9 ± 4.6
Pao diastolic, mm Hg	93.0 ± 4.4	86.8 ± 3.1	88.5 ± 3.8
Pao mean, mm Hg	109.2 ± 4.8	104.2 ± 3.2	104.8 ± 3.9
Cardiac output, ml/min	73.8 ± 4.5	55.9 ± 3.8	59.8 ± 4.7
Stroke volume, μl	239.1 ± 14.4	176.9 ± 11.5	196.3 ± 13.7
End-diastolic volume, μl	384.4 ± 25.5	512.7 ± 25.7	424.8 ± 24.2*
End-systolic volume, μl	180.7 ± 25.4	328.7 ± 30.9	261.9 ± 24.3*
Ejection fraction, %	66.8 ± 5.2	37.7 ± 3.4	49.6 ± 3.6*
dV/dt max, ml/s	8.7 ± 0.6	7.4 ± 0.7	8.1 ± 0.5
LV volume at dP/dt max, μl	371.5 ± 25.8	464.3 ± 29.0	406.7 ± 25.0*
LV volume at dP/dt min, μl	173.8 ± 23.4	317.3 ± 30.4	250.0 ± 23.6*
ESPVR slope, mmHg/μl	0.51 ± 0.11	0.73 ± 0.19	0.62 ± 0.18
Tau, ms	10.8 ± 1.4	11.7 ± 1.4	12.8 ± 2.2

Values are mean ± SEM. Dunnett's versus vehicle: *$p < 0.05$.

Cmpd43 = Compound 43; ESPVR = end-systolic pressure-volume relationship; LV = left ventricular; Pao = aortic pressure.

increase in scar distension and compliance. E_{11} strains for the 1 mg/kg and 10 mg/kg Cmpd43 treatment groups approached levels achieved with sham hearts, indicating stiffer scarring in this direction. On average, smaller scar strains were obtained with 10 mg/kg Cmpd43 versus the 1 mg/kg treatment. As shown in **Figure 6D**, in the E_{22} direction (longitudinal axis), sham mice showed little change in strains (stiff myocardium), and vehicle showed the greatest increase in strains. Treatment with 1 mg/kg Cmpd43 produced a profile that closely resembled that of vehicle. At the 10 mg/kg dose, the profile showed an intermediate effect between sham and vehicle, suggesting an increase in infarct stiffness relative to vehicle.

The capacity of Cmpd43 to improve LV and infarct scar remodeling post-MI was also evaluated in the rat model. An IR design was used to reflect the clinical scenario because reperfusion strategies are used post-MI. LV PV curves (**Figure 7A**) obtained for the MI vehicle group showed an expected rightward shift compared with sham. The PV curve obtained with 10 mg/kg Cmpd43 was left-shifted relative to vehicle, indicating smaller chamber volumes. A trend toward a reduced heart weight/body weight ratio was observed with Cmpd43 treatment relative to the MI vehicle group and was comparable to the heart weight/body weight ratio of sham (**Figure 7B**). The MI vehicle group showed a 33% increase in mean LV end-diastolic volume relative to sham. Cmpd43 10 mg/kg decreased LV end-diastolic volume relative to vehicle by 17% (**Figure 7C**) ($p < 0.05$). As shown in **Figure 7D**, infarcted rats treated with vehicle showed a mean ejection fraction of 38%, whereas noninfarcted sham hearts had an ejection fraction average of 67%. Treatment with Cmpd43 yielded a statistically significant relative improvement in ejection fraction of 32% versus vehicle (12% absolute increase; $p < 0.05$). **Table 1** summarizes the various hemodynamic parameters measured in the study. Regional measurements of viable myocardium relative to infarct scar tissue were made transmurally across the infarct wall (i.e., from epicardium to endocardium) (**Figure 7E**). Preservation of myocardium was observed with Cmpd43 at the proximal MI region (nearest the ligature; 34% relative increase vs. vehicle; $p < 0.01$), at the mid-MI wall (44% relative increase vs. vehicle; $p < 0.001$), and at the distal MI region (35% relative increase vs. vehicle; $p < 0.01$). No statistically significant differences in wall thickness between vehicle- and Cmpd43-treated rats were observed in any region of the MI (Online Figure 5). Noninfarcted sham rats had 100% viable transmural walls (data not shown).

DISCUSSION

Activation of the acute inflammatory response following MI facilitates the onset of wound healing and scar formation in the heart. Dysregulation and/or prolongation of the inflammatory response can lead to additional tissue damage, worsened LV function, and eventual decompensation, leading to HF. In this regard, activation of the resolution process is critical for restoring damaged tissue to a non-inflamed healed state. Pharmacological strategies to stimulate inflammation resolution may thus speed healing and limit adverse post-MI changes in cardiac structure and function. Our findings demonstrated that targeted stimulation of FPR1/2 with Cmpd43 enhanced immune responses that drive inflammation resolution. In vivo, Cmpd43 protected the heart from ischemic injury and prevented the deterioration of cardiac function post-MI.

Macrophage phagocytosis of apoptotic and necrotic cells was shown to enable wound healing and to potentiate post-MI inflammation resolution (23,24). In WT mice, Cmpd43 stimulated robust phagocytosis of zymosan particles; the activity was largely attributed to FPR2, because no enhancement in zymosan clearance was observed in FPR2-deficient macrophages. These data are consistent with impairments in phagocytosis of peritoneal bacteria observed in a sepsis model that used FPR2-deficient mice (25). Interestingly, when phagocytosis experiments were carried out with FPR1-deficient macrophages, a decrease in potency was observed, which suggested

the partial involvement of FPR1 in phagocytosis. Activated phagocytes release reactive oxygen species (oxidative burst) into the ingested phagosome (19). Oxidative burst profiles obtained with parental HL-60 cells and those deficient in FPR1 or FPR2 revealed similar activity patterns after Cmpd43 exposure to those shown with peritoneal macrophages (i.e., no response with FPR2 deficiency and a slightly right-shifted response with FPR1 deficiency). Cmpd43 also readily stimulated HL-60 cell chemotaxis, whereas FPR1- and FPR2-deficient lines showed severely diminished responses. These results are in line with published reports that described the involvement of FPR1/2 in leukocyte chemotaxis (12,26,27).

The concentration-dependent effects of Cmpd43 on intracellular signaling of FPR1/2 via Gαi and Gαo proteins confirmed the known coupling of these receptors to the Gi family (10,28,29). Following activation of Gαi/o proteins, the dissociated Gβγ subunits engage downstream effectors, leading to release of calcium from intracellular stores and protein kinase C activation, a process believed to play a role in superoxide production and chemotaxis (30,31). Beyond the Gi family, engagement of Gα12 and Gα13 proteins was also observed upon stimulation with Cmpd43, for both FPR1 and FPR2. Such coupling of FPRs to Gα12 and Gα13 pathways was previously suggested based on the effect of Gα12/Gα13 dominant-negative constructs on cell polarity induced by stimulation of HL-60 cells with the FPR1 ligand fMLP (32). In addition to promoting activation of Gαi/o and Gα12/13 proteins, Cmpd43 stimulated FPR1/2-mediated recruitment of β-arrestins. A variety of FPR1/2 agonists are known to recruit β-arrestin (13,33). A noncanonical role for β-arrestin in leukocyte function, to include cell migration and infiltration, has been described and might be relevant to key functions attributed to FPR1/2 action (34). In human neutrophils, a selective FPR2 agonist with impaired β-arrestin recruitment properties was unable to stimulate chemotaxis (35). In HL-60 cells, targeted knockdown of β-arrestin-1 using short hairpin RNA-containing viral particles displayed a clear defect in chemotaxis towards fMLP (36). These observations demonstrate the importance of β-arrestin in leukocyte trafficking, in which impairments in this signaling pathway might disrupt important leukocyte responses during wound healing.

IL-10 has been described as a potent anti-inflammatory cytokine with clear links to the resolution of myocardial inflammation (37). In vitro treatment of SAA-activated peritoneal macrophages with Cmpd43 resulted in concentration-dependent increases in IL-10 mRNA levels, which were abolished in the absence of FPR2. Relevant to the present study, it has been reported that increases in IL-10 via short-term exogenous administration attenuated LV remodeling and infarct wall thinning post-MI (38). These improvements were preceded by early decreases in proinflammatory cytokines (IL-6, tumor necrosis factor-α, and others) in the myocardium. In the present study, Cmpd43 also reduced IL-6 mRNA in SAA-activated macrophages, which indicated a drive toward the resolution of inflammation. Collectively, these data support the concept that early macrophage FPR cytokine regulation, and, in particular, FPR2, achieved with Cmpd43 could lead to favorable effects on downstream LV remodeling post-MI. It was further demonstrated that early changes in macrophage phenotype could be evoked by Cmpd43 in post-MI cardiac tissue. An increase in proresolution $CD206^{+}$ macrophages was noted in the myocardium of mice assessed approximately 3 days post-MI. This was accompanied by increased expression of the proresolution marker, arginase-1, at the border zone of the infarct. These findings were consistent with the capacity of Cmpd43 via FPRs to stimulate proresolution macrophages during wound repair after MI. Importantly, enhanced expression of resolution markers achieved with endogenous ligands for FPR2 in the mouse heart has been reported to correlate with improved myocardial healing and LV function post-MI (8,9,39).

Long-term treatment with Cmpd43 improved cardiac structure and function relationships in both the mouse permanent coronary artery occlusion and rat IR MI models. In the mouse, Cmpd43 attenuated adverse LV remodeling following permanent LAD artery occlusion as indicated by reduced LV chamber areas and left-shifted PV curves. This was accompanied by a reduction in infarct scar size and preservation of infarct wall thickness compared with vehicle. In addition, passive 2-dimensional strains indicated increased scar stiffness with Cmpd43 treatment (E_{11} at all doses; E_{22} at high dose). Following IR injury in the rat, Cmpd43 attenuated LV chamber dilatation, improved systolic LV function, and increased viable myocardium levels across the infarct wall, which indicated that Cmpd43 was associated with the preservation of functional myocardium within the infarct scar. Considering these findings, the following observations merit attention. First, Cmpd43 treatment was started 24 to 48 h post-MI, which coincides with the peak of early

inflammation that involves neutrophils and proinflammatory monocytes (40). As such, the inflamed and ischemic tissue might represent an opportunistic site of action for FPR-targeted therapy. Second, the early increase in proresolution macrophages in the myocardium and infarct border zone suggested that macrophage polarization occurred with FPR1/2 agonism. These changes were predicted to increase wound healing activity early post-MI, leading to improved structure and/or function outcomes. As previously stated, early stimulation of a proresolution phenotype in the heart has been shown to diminish myocardial inflammation and reduce deterioration in LV function (8,9). The present study provided further direct evidence in support of proresolution strategies to treat post-MI injury and prevent HF development. Our studies were interventional in nature because treatment was given after MI. This was unique among the various reports that used FPR agonists to affect outcome post-MI (8-10,41,42). Although previous studies pre-treated with an agonist or provided it at the time of ischemic injury, our studies showed the impact of intervention within days following MI. The incorporation of an additional assessment of the impact of Cmpd43 treatment initiated in the first few hours post-MI would have been informative. The impact of timing of intervention post-MI, and, in particular, delayed intervention, on outcome remains to be addressed.

The effects of synthetic small molecule agonists of FPR1/2, including Cmpd43, on myocardial injury and infarction have been described (10). In a study by Qin et al. (10), mice subjected to IR were treated parenterally with Cmpd43 starting 24 h before ischemia and daily for 7 days thereafter. Cmpd43 was ineffective in reducing early cardiac necrosis and inflammation, and was unable to attenuate LV remodeling 7 days post-IR injury. In our study, therapeutic benefit with Cmpd43 was achieved in scar structure and cardiac function endpoints in mouse and rat models of MI. However, distinct differences between these 2 studies are worth highlighting. In our present study: 1) treatment was 10 mg/kg given orally by gavage versus 50 mg/kg via intraperitoneal administration; 2) treatment was started 24 to 48 h post-ischemia versus 24 h before ischemia; 3) treatment duration lasted up to 28 days post-MI versus 7 days; and 4) mouse MI models were different (IR vs. permanent coronary artery occlusion). As stated earlier, the interventional approaches used in the present study to respond to acute MI could be applicable to the clinical setting. Qin et al. (10) showed that an alternate FPR1/2 dual agonist (Cmpd17B) (10) improved systolic function and reduced proinflammatory gene expression profiles in the infarct zone 28 days post-MI, which aligned with Cmpd43 activity described in this study. Cmpd17B results coupled with data from this report support the concept that FPR1/2 dual agonism improves LV structure and function post-MI.

The present findings also point to a process of early changes in cardiac macrophage phenotype, whereby FPR1/2 dual agonism evokes a more "resolution competent" cell type. This process is suggested to increase macrophage phagocytic activity within and vicinal to the MI to enhance clearance of necrotic debris. The enhanced clearance of necrotic material could enable wound healing and productive scar formation post-MI. In addition, an enhancement in homing of monocyte macrophages to the site of injury would also likely serve to increase the pool of proresolution macrophages for tissue repair. The early changes in the macrophage profile ultimately led to improvements in scar maturation and overall outcome. A recent study by Heo et al. (43) also revealed a role for FPR2 activation in recruitment of circulating proangiogenic cells into the infarcted myocardium that led to myocardial protection post-MI. These findings indicate a beneficial, yet more complex, role of FPRs in myocardial wound healing.

CONCLUSIONS

In these studies, we demonstrate that FPR1/2 dual agonism using Cmpd43 stimulates prophagocytic and prochemotactic cellular responses essential for proresolution function. As a result, Cmpd43 favorably mitigates adverse LV remodeling and promotes optimal myocardial healing in mouse and rat models of MI, leading to favorable changes in chamber function. Direct therapeutic targeting of FPRs, and in particular, FPR2, may thus represent a viable strategy to prevent HF development in patients following an MI. Clinical studies with FPR agonists will help to address this exciting potential.

ACKNOWLEDGMENTS Editorial support was provided by Geraint Owens, PhD, of Chameleon Communications International Ltd, with funding from Bristol-Myers Squibb.

ADDRESS FOR CORRESPONDENCE: Dr. Ricardo A. Garcia, Bristol-Myers Squibb Company, 311 Pennington-Rocky Hill Road, Pennington, New Jersey 08534. E-mail: Ricardo.Garcia@bms.com.

PERSPECTIVES

COMPETENCY IN MEDICAL KNOWLEDGE: Our studies demonstrated the beneficial effects of long-term FPR activation with Cmpd43 in the setting of post-MI injury. Treatment resulted in the promotion of a proresolution macrophage profile (cellular function, cytokine responses, and gene signatures) and an enhanced understanding of the signaling profile in model cell culture systems. Importantly, treatment improved LV structure and function relationships in rodent MI models (permanent coronary artery occlusion and IR injury), highlighting the importance of the resolution process in post-MI healing.

TRANSLATIONAL OUTLOOK: Demonstration of efficacy with long-term FPR agonist treatment in animal models of MI provides fundamental and essential proof of principle for future evaluation of this mechanism in the post-MI patient population.

REFERENCES

1. Writing Group Members, Mozaffarian D, Benjamin EJ, et al. Heart disease and stroke statistics-2016 update: a report from the American Heart Association. Circulation 2016;133:e38–360.

2. Serhan CN, Chiang N, Dalli J. The resolution code of acute inflammation: novel pro-resolving lipid mediators in resolution. Semin Immunol 2015;27:200–15.

3. Hammerman H, Kloner RA, Hale S, Schoen FJ, Braunwald E. Dose-dependent effects of short-term methylprednisolone on myocardial infarct extent, scar formation, and ventricular function. Circulation 1983;68:446–52.

4. Roberts R, DeMello V, Sobel BE. Deleterious effects of methylprednisolone in patients with myocardial infarction. Circulation 1976;53:I204–6.

5. Saito T, Rodger IW, Hu F, Robinson R, Huynh T, Giaid A. Inhibition of COX pathway in experimental myocardial infarction. J Mol Cell Cardiol 2004;37:71–7.

6. Kimmel SE, Berlin JA, Reilly M, et al. Patients exposed to rofecoxib and celecoxib have different odds of nonfatal myocardial infarction. Ann Intern Med 2005;142:157–64.

7. Serhan CN, Krishnamoorthy S, Recchiuti A, Chiang N. Novel anti-inflammatory-pro-resolving mediators and their receptors. Curr Top Med Chem 2011;11:629–47.

8. Kain V, Ingle KA, Colas RA, et al. Resolvin D1 activates the inflammation resolving response at splenic and ventricular site following myocardial infarction leading to improved ventricular function. J Mol Cell Cardiol 2015;84:24–35.

9. Kain V, Liu F, Kozlovskaya V, et al. Resolution agonist 15-epi-lipoxin A4 programs early activation of resolving phase in post-myocardial infarction healing. Sci Rep 2017;7:9999.

10. Qin CX, May LT, Li R, et al. Small-molecule-biased formyl peptide receptor agonist compound 17b protects against myocardial ischaemia-reperfusion injury in mice. Nat Commun 2017;8:14232.

11. Burli RW, Xu H, Zou X, et al. Potent hFPRL1 (ALXR) agonists as potential anti-inflammatory agents. Bioorg Med Chem Lett 2006;16:3713–8.

12. Sogawa Y, Shimizugawa A, Ohyama T, Maeda H, Hirahara K. The pyrazolone originally reported to be a formyl peptide receptor (FPR) 2/ALX-selective agonist is instead an FPR1 and FPR2/ALX dual agonist. J Pharmacol Sci 2009;111:317–21.

13. Forsman H, Onnheim K, Andreasson E, Dahlgren C. What formyl peptide receptors, if any, are triggered by compound 43 and lipoxin A4? Scand J Immunol 2011;74:227–34.

14. Salahpour A, Espinoza S, Masri B, Lam V, Barak LS, Gainetdinov RR. BRET biosensors to study GPCR biology, pharmacology, and signal transduction. Front Endocrinol (Lausanne) 2012;3:105.

15. Dufton N, Hannon R, Brancaleone V, et al. Anti-inflammatory role of the murine formyl-peptide receptor 2: ligand-specific effects on leukocyte responses and experimental inflammation. J Immunol 2010;184:2611–9.

16. Liang TS, Wang JM, Murphy PM, Gao JL. Serum amyloid A is a chemotactic agonist at FPR2, a low-affinity N-formylpeptide receptor on mouse neutrophils. Biochem Biophys Res Commun 2000;270:331–5.

17. Brandenburg LO, Konrad M, Wruck C, Koch T, Pufe T, Lucius R. Involvement of formyl-peptide-receptor-like-1 and phospholipase D in the internalization and signal transduction of amyloid beta 1-42 in glial cells. Neuroscience 2008;156:266–76.

18. Planaguma A, Domenech T, Jover I, et al. Lack of activity of 15-epi-lipoxin A(4) on FPR2/ALX and CysLT1 receptors in interleukin-8-driven human neutrophil function. Clin Exp Immunol 2013;173:298–309.

19. Forman HJ, Torres M. Reactive oxygen species and cell signaling: respiratory burst in macrophage signaling. Am J Respir Crit Care Med 2002;166:S4–8.

20. Gallagher R, Collins S, Trujillo J, et al. Characterization of the continuous, differentiating myeloid cell line (HL-60) from a patient with acute promyelocytic leukemia. Blood 1979;54:713–33.

21. Bartekova M, Radosinska J, Jelemensky M, Dhalla NS. Role of cytokines and inflammation in heart function during health and disease. Heart Fail Rev 2018;23:733–58.

22. ter Horst EN, Hakimzadeh N, van der Laan AM, Krijnen PA, Niessen HW, Piek JJ. Modulators of macrophage polarization influence healing of the infarcted myocardium. Int J Mol Sci 2015;16:29583–91.

23. Lambert JM, Lopez EF, Lindsey ML. Macrophage roles following myocardial infarction. Int J Cardiol 2008;130:147–58.

24. Wan E, Yeap XY, Dehn S, et al. Enhanced efferocytosis of apoptotic cardiomyocytes through myeloid-epithelial-reproductive tyrosine kinase links acute inflammation resolution to cardiac repair after infarction. Circ Res 2013;113:1004–12.

25. Gobbetti T, Coldewey SM, Chen J, et al. Nonredundant protective properties of FPR2/ALX in polymicrobial murine sepsis. Proc Natl Acad Sci U S A 2014;111:18685–90.

26. Dalli J, Montero-Melendez T, McArthur S, Perretti M. Annexin A1 N-terminal derived peptide ac2-26 exerts chemokinetic effects on human neutrophils. Front Pharmacol 2012;3:28.

27. Liu M, Chen K, Yoshimura T, et al. Formylpeptide receptors are critical for rapid neutrophil mobilization in host defense against Listeria monocytogenes. Sci Rep 2012;2:786.

28. Le Y, Murphy PM, Wang JM. Formyl-peptide receptors revisited. Trends Immunol 2002;23:541–8.

29. Harada M, Habata Y, Hosoya M, et al. N-Formylated humanin activates both formyl peptide receptor-like 1 and 2. Biochemi Biophys Res Commun 2004;324:255–61.

30. Rabiet MJ, Huet E, Boulay F. The N-formyl peptide receptors and the anaphylatoxin C5a receptors: an overview. Biochimie 2007;89:1089–106.

31. Ye RD, Boulay F, Wang JM, et al. International Union of Basic and Clinical Pharmacology. LXXIII. Nomenclature for the formyl peptide receptor (FPR) family. Pharmacol Rev 2009;61:119–61.

32. Xu J, Wang F, Van Keymeulen A, et al. Divergent signals and cytoskeletal assemblies regulate

self-organizing polarity in neutrophils. Cell 2003;114:201–14.

33. Krishnamoorthy S, Recchiuti A, Chiang N, et al. Resolvin D1 binds human phagocytes with evidence for proresolving receptors. Proc Natl Acad Sci U S A 2010;107:1660–5.

34. Sharma D, Parameswaran N. Multifaceted role of beta-arrestins in inflammation and disease. Genes Immun 2015;16:499–513.

35. Gabl M, Holdfeldt A, Sundqvist M, Lomei J, Dahlgren C, Forsman H. FPR2 signaling without beta-arrestin recruitment alters the functional repertoire of neutrophils. Biochem Pharmacol 2017;145:114–22.

36. Gera N, Swanson KD, Jin T. β-Arrestin 1-dependent regulation of Rap2 is required for fMLP-stimulated chemotaxis in neutrophil-like HL-60 cells. J Leukoc Biol 2017;101:239–51.

37. Jung M, Ma Y, Iyer RP, et al. IL-10 improves cardiac remodeling after myocardial infarction by stimulating M2 macrophage polarization and fibroblast activation. Basic Res Cardiol 2017;112:33.

38. Krishnamurthy P, Rajasingh J, Lambers E, Qin G, Losordo DW, Kishore R. IL-10 inhibits inflammation and attenuates left ventricular remodeling after myocardial infarction via activation of STAT3 and suppression of HuR. Circ Res 2009;104:e9–18.

39. Halade GV, Kain V, Serhan CN. Immune responsive resolvin D1 programs myocardial infarction-induced cardiorenal syndrome in heart failure. FASEB J 2018;32:3717–29.

40. Nahrendorf M, Pittet MJ, Swirski FK. Monocytes: protagonists of infarct inflammation and repair after myocardial infarction. Circulation 2010;121:2437–45.

41. D'Amico M, Di Filippo C, La M, et al. Lipocortin 1 reduces myocardial ischemia-reperfusion injury by affecting local leukocyte recruitment. FASEB J 2000;14:1867–9.

42. Dalli J, Consalvo AP, Ray V, et al. Proresolving and tissue-protective actions of annexin A1-based cleavage-resistant peptides are mediated by formyl peptide receptor 2/lipoxin A4 receptor. J Immunol 2013;190:6478–87.

43. Heo SC, Kwon YW, Jang IH, et al. Formyl peptide receptor 2 is involved in cardiac repair after myocardial infarction through mobilization of circulating angiogenic cells. Stem Cells 2017;35:654–65.

KEY WORDS agonist, Compound 43, formyl peptide receptor, heart failure, myocardial infarction

APPENDIX For an expanded Methods section and supplemental figures, please see the online version of this paper.